Lacustrine shale oiliness influenced by diabase intrusions in the Paleogene Funing Formation, Subei Basin, China

Biao Sun, Xiaoping Liu, Jie Liu, Qidong Liu, Hongliang Duan, Shili Liu, Ming Guan, Tian Liu, Zuxian Hua, Kai Sheng, Yujie Xing

PII: S1995-8226(23)00138-3

DOI: https://doi.org/10.1016/j.petsci.2023.05.013

Reference: PETSCI 542

To appear in: *Petroleum Science*

Received Date: 29 August 2022

Revised Date: 30 January 2023

Accepted Date: 18 May 2023

Please cite this article as: Sun, B., Liu, X., Liu, J., Liu, Q., Duan, H., Liu, S., Guan, M., Liu, T., Hua, Z., Sheng, K., Xing, Y., Lacustrine shale oiliness influenced by diabase intrusions in the Paleogene Funing Formation, Subei Basin, China, *Petroleum Science* (2023), doi: https://doi.org/10.1016/j.petsci.2023.05.013.

Lacustrine shale oiliness influenced by diabase intrusions in the Paleogene Funing Formation, Subei Basin, China

Biao Sun [a,b], Xiaoping Liu [a,b*], Jie Liu [c], Qidong Liu [d], Hongliang Duan [d], Shili Liu [d], Ming Guan [a,b], Tian Liu [a,b], Zuxian Hua [a,b], Kai Sheng [a,b], Yujie Xing [d]

a. State Key Laboratory of Petroleum Resources and Prospecting, China University of Petroleum (Beijing), Beijing, 102249, China.

b. College of Geosciences, China University of Petroleum (Beijing), Beijing, 102249, China.

c. International Petroleum Exploration and Production Corporation, SINOPEC, Beijing 100029, China.

d. Research Institute of Exploration and Development, SINOPEC Jiangsu Oilfield Company, Jiangsu 225009)

* Corresponding author. College of Geosciences, China University of Petroleum (Beijing), Beijing 102249, China

E-mail: liuxiaoping@cup.edu.cn (X. Liu)

ABSTRACT

The research on the correlation between hydrocarbon accumulations and magmatic activities has always attracted aroused much wide attention. Existing research has primarily the hydrocarbon generations capability of source rocks and the quality of reservoirs by diabase intrusions. whereas, rare systematic research has been conducted on the oiliness and enrichment mechanism. To be specific, the diabase intrusive zone, the contact metamorphic zone and the normal shale zone of the Funing Formation in the Gaoyou Sag, Subei Basin were taken as the object of this study. Moreover, in this study, the hydrocarbon generation quality, reservoir quality, and oil-bearing quality of diabase-metamorphic zone-normal shale were evaluated using X-ray diffractions, argon ion polishing-field emission scanning electron microscope, energy spectrum, rock slice/light-sheet microscopic observations, organic geochemical tests, N_2 gas adsorption and 2-D NMR tests .The results indicated that the intrusive zone, the metamorphic zone, and the normal zone were formed in order by the degree of effect of diabase intrusions. Secondly, the oil content of different parts exhibited significant heterogeneity due to the baking effect of diabase, and the metamorphic zone had the significantly better oil-bearing nature than the intrusive zone. Lastly, a distribution model was proposed for the diabase intrusive zone-metamorphic zone-normal surrounding rock zone.

Keywords Shale reservoirs, Diabase intrusion, Oiliness, Funing Formation

1 Introduction

Since volcanic oil and gas reservoirs in the San Joaquin Basin in California were initially discovered at the end of the 19th century, oil and gas reservoirs displays associated with magmatic activities have been discovered in over 300 sedimentary basins of more than 100 regions (Thomaz Filho et al., 2008; Rodriguez Monreal et al., 2009; Spacapan et al., 2018), and breakthroughs have been achieved in volcanic oil and gas exploration in Songliao, Bohai Bay, Junggar, and Santanghu basins in China (Zou

et al., 2008). The research on the correlation between magmatic activity and hydrocarbon accumulations has always aroused wide attention, whereas the existing exploration and research results have been largely concentrated in volcanic reservoirs, with relatively few intrusive rocks. The correlation between intrusive reservoirs and intrusive rocks, as well as the transformation of conventional oil and gas reservoirs. However, the mechanism of the shale oil source storage system (Xu et al., 2015; Yu et al., 2016; Ye et al., 2022;) and shale oil enrichments has been rarely investigated.

Diabase intrusions affects the hydrocarbon generation of organic matter, while changing the geochemical characteristics of hydrocarbon products. The degree and mechanism of the effect of diabase intrusion on the on lacustrine shale oil should be investigated. The effect of diabase intrusion on the hydrocarbon generations of organic matter has been studied for a long period. Extensive studies have suggested that vitrinite reflectance (Ro) of the shale affected by diabase intrusions is significantly higher than that of the shale far away from diabase. Diabase intrusions takes on a positive significance to in the thermal evolution of organic matter. With the distance from the source rocks to the diabase intrusions, the total organic carbon content (TOC), chloroform pitch "A", S_1, S_2 and other parameters have changed regularly, except for the sudden increase of the Ro, thus suggesting the intensity of organic matter hydrocarbon generation is significantly affected by diabase intrusions (de Souza et al., 2019; Li et al., 2020b; Martins et al., 2020; Teixeira et al., 2020). The influence and modification of magma intrusion on hydrocarbon generation process and hydrocarbon products of organic shale will inevitably have an important impact on the occurrence and flow of shale oil, and the hydrothermal fluid carried by magma carries physical and chemical modifications to the surrounding shale reservoir, but the degree and mechanism of transformation need to be studied urgently (Wu et al., 2011; Koltzer et al., 2017; MA et al., 2019; Chen et al., 2021; LIU et al., 2021; Shu et al., 2021).

Diabase intrusion is very common in lacustrine shale, and shale oil is active in diabase distribution areas. The Subei Basin, the Bohai Bay Basin, the Songliao Basin, the Santanghu Basin and other continental strata have developed diabase intrusions, and oil and gas reservoirs have been discovered in diabase and its surrounding rocks (Liu

et al., 2016; Du et al., 2019; Liu et al., 2019; Rong et al., 2021). With the Subei Basin as an example, diabase intrusions in the Paleogene are have been extensively distributed, taking up a distribution area of over 1000 km^2, with the major distribution in Gaoyou, Jinhu, Qintong, Haian sag, as well as Baiju sag. The focus of this study was placed on the petrological, geochemical, and oil-bearing characteristics of the intrusive diabase and metamorphic shale reservoirs in the study area. Subsequently, the distribution characteristics of the shale oiliness in different zones affected by diabase intrusions were analyzed. Lastly, an evolution model was proposed for the diabase-metamorphic reservoir complex. In this study, a useful analogy was presented to explore intrusive metamorphic reservoirs, which also provides an important reference for other regions with similar geological backgrounds in the world. Shale oil strata (continental and marine) in many basins in the world have developed different types of magmatic intrusive rocks, such as Gunnedah Basin, Australia (Othman et al., 2001) and Sverdrup Basin, Arctic Canada (Goodarzi et al., 2019), among which diabase intrusion is very common. China is located on the Eurasian plate, adjacent to the Pacific plate to the east, the influence of deep magmatic activity in the formation of continental fault basins is particularly prominent. This study focuses on the influence of deep magmatic intrusion activity on shallow sedimentary strata, especially shale oil strata, which brings both energy and material effects to shale strata, so this study is of great significance for revealing the organic and inorganic interaction between magmatic activity and shale oil strata, and expands the research field of shale oil formation enrichment theory.

2 Geological settings

The area of the Subei Basin is nearly 3.6×10^4 km^2, which is the largest Mesozoic-Cenozoic basin in southeastern China. This area extends eastward to the Yellow Sea (**Fig. 1a**) (Liu et al., 2021), and the structural units of the Subei basin comprises three structures (**Fig. 1b**) (Cheng et al., 2019). The Gaoyou Sag is located in the center of the Dongtai Depression, and it is a skip-shaped rift formed by the different fault blocks under Yizheng movement and the Wubao movement. The sag is cut into

sub-level structural units, i.e., it is split into the southern fault step belt, the central deep depression belt , as well as the northern slope belt (**Fig. 1**) (Liu et al., 2019).

Four formations have been developed in the Gaoyou Sag (including the Taizhou formation, the Funing formation, the Dainan formation and the Sanduo formation). A total of 11 third-order sequences have been developed in the first-order sequence framework. To be specific the second and fourth members of Funing formation are deep lakes, and the lithology is largely dark shale. The structural activities are frequent in the Gaoyou Sag, thus resulting in the development of diabase intrusions. The occurrences of diabase are mostly dyking and bedrocks. The thickness of a single layer ranges from a few meters to over 200 meters. The intrusive horizon is dominated by the Funing Formation that originates from multiple tectonic movements (Gao et al., 2018). The north slope of the Gaoyou Sag takes up an area of nearly 1.3×10^4 km^2, and it is the main site of diabase intrusions (**Fig. 1**).

Fig. 1. Location and tectonic units of the study area in Subei Basin (a), Location of Subei Basin Division of Basic Structural Units of Subei Basin (b), Areal map showing the substructural units and diabase distribution in the Gaoyou sag (c).

Fig. 2. Stratigraphic characteristics, sequence stratigraphic framework and sample location of well Z1 in the Gaoyou Sag

3 Samples and experiments

3.1 Samples

In this study, 11 core samples were collected from the well Z1 in the Gaoyou Sag, Subei Basin (**Table 1**). The Funing formation refers to a set of organic-rich lacustrine shale formations. The location of the well Z1 is illustrated in **Fig. 1c**. The samples from the well Z1 were taken at the depths from 1568.47 m to 1790.18 m (**Fig. 2**). A series of tests were performed out on the above samples (e.g., thin sections observations, FIB-SEM, X-ray, TOC, N_2 gas adsorption analyses and 2-D NMR analysis).

The NMR experiments were all performed by the Accumulation and Development of Continental Oil and Gas Key laboratory of Education Ministry, Northeast Petroleum University.

Table 1 Samples information, Funing Formation, Subei Basin

Sample	Depth/m	Member	Style	Lithology
1	1568.47	Paleogene	Core	hornfels
2	1571.87	Paleogene	Core	hornfels
3	1580.78	Paleogene	Core	hornfels
4	1602.68	Paleogene	Core	diabase
5	1603.64	Paleogene	Core	diabase
6	1607.37	Paleogene	Core	diabase
7	1608.87	Paleogene	Core	diabase
8	1657.65	Paleogene	Core	slate
9	1664.82	Paleogene	Core	slate
10	1778.73	Paleogene	Core	shale
11	1790.18	Paleogene	Core	shale

3.2 Experiments

3.2.1 Thin sections and SEM observation

Ilion 697 was adopted to polish the shale samples with argon ion for preparing the shale samples. The polishing time was nearly 2 h. The polished surface of the

samples was sprayed with a thin layer of carbon to enhance the conductivity of the shale surface. The pore characteristics of the processed shale samples were identified under the ZEISS Crossbeam 540 (Carl Zeiss Industrial Metrology) field emission scanning electron microscope. The minimum observable aperture was 2 nm. The probe combined a secondary electron probe and a backscattered electron probe. The secondary electron probe was primarily adopted to characterize the morphology of minerals, while the backscattered electron probe was employed to observe the pores.

3.2.2 N_2 gas adsorption analyses

N_2 gas adsorption and desorption examinations were performed using a Micromeritics ASAP 2460 surface area and pore volume analyzer. A total of 11 specimens were screened to gain the grain measures of 40–60 mesh before drying in a vacuum oven at 150 for 8 h (Guan et al., 2020). The mesopores (2–50 nm) and several macropores (50 nm) were defined using the N_2 gas adsorption evaluation, and the measurements were performed at 25 (based on standard SY/T 6154–1995, China Petroleum Industry Standards) with a relative pressure (p/p_0) range of 0.01–0.995. In accordance with the test, the surface area and total pore volume were expressed using a combination of nonlocal-density functional theory (NLDFT) and density functional theory (DFT) models (Aljamaan et al., 2017; Annuar et al., 2021).

3.2.3 NMR experiments

The samples with a mass of nearly 30 g were taken, and two-dimensional (2D) nuclear magnetic resonance experiments were performed at 20 . The NMR test parameters were: echo time (TE), 0.07 ms; waiting time (TW),1000 ms; number of echos (NECH), 6000; number of scans (NS), 32. After the instrument was calibrated to detect ^{1}H-containing compounds, the first step is to perform T_2 detection to obtain the total amount of ^{1}H-containing compounds in the shale sample. Subsequently, T_1-T_2 2D nuclear magnetic detection was performed to obtain a 2D spectrum. The of the content

of different compounds was quantitatively divided.

4 Results

4.1 Mineralogy and organic geochemistry

The high-grade metamorphic rocks of the Funing Formation in the study area were hornfels, which primarily comprise clay (7.4–26.8%), quartz (0.6–17.5%), feldspar (0.0–16.4%), as well as carbonate (10.3–41.9%) (**Table 2**). The hornfels exhibit a typical blastic texture (**Fig. 3a**), and some hornfels was chlorinated (**Fig. 3b**) in the study area. The hornfels comprised metamorphic minerals, especially augite.

The low-grade metamorphic rocks were primarily low metamorphic slate. The slate comprised clay (16.4–25.7%), quartz (0.6–2.4%), feldspar (3.8–24.5%) and carbonate (11.3–36.6%) (**Table 2**). The slate usually far away from the intrusive diabase was characterized by the fissure structure and horizontal micro-layers, and a wide variety of slabs were developed (**Fig. 3c**). Moreover, directional microstructures were generated when part of the force was applied. In addition, microcracks (**Fig. 3d**), sericitization and cliticization occurred. Some minerals indicated the degree of metamorphisms (e.g., chlorites) The slate was 7–8%, the surface of the slate was completely chlorinated (**Fig. 3e**), and the chlorites grew in the clay minerals (**Fig. 3f**).

In general, the none metamorphic rocks were shale. The shale comprised clay (30.9–37.6%), quartz (0.8–4.1%), feldspar (17.2–33.2%) and carbonate (25.5–32.9%) (**Table 2**). The normal zone usually far away from the intrusive diabase is characterized by pelitic texture (**Fig. 3g**); it contained a considerable number of calcites (**Fig. 3h**); it was relatively dense (**Fig. 3i**).

The results show that the vertical distribution characteristics of TOC and Ro have obvious heterogeneity (**Table 3**). The TOC of the samples ranging from 0.04% to 2.04% with an average of 0.80% The Ro vary from 0.52% to 2.20%, indicating that the sample has low-maturity- high-maturity characteristics.

Fig. 3. Cores, SEM images, and photomicrographs showing lithology and porosities of the diabase and contact shale.

Well, Z1, 1571.87 m, hornfels, filled with chlorite (a), Well, Z1, 1571.87 m, chlorite and augite (b), Well, Z1, 1580.78 m, hornfels, organic matter and augite (c), Well, Z1, 1657.65 m, gray-black layered slate with high angle cracks filled with calcite (d), Well, Z1, 1657.65 m, chlorinated slate (e), Well, Z1, 1657.65 m, chlorite in slate (f), Well, Z1, 1778.93 m, shale with pelitic texture (g), Well, Z1, 1778.93 m, shale containing a lot of calcites (h), Well, Z1, 1778.93 m, shale is relatively dense (i).

Table 2 Mineral composition of samples, Funing Formation, Subei Basin

Sample	Mineral compositions/%								Clay minerals/%			
	Clay	Quartz	Feldspar	Calcite	Dolomite	Siderite	Ankerite	Augite	I/S	I	K	C
1	7.4	17.5	0.0	34.6	0.0	12.1	11.7	0.0	66.0	19.0	7.0	8.0
2	18.8	1.3	9.2	3.5	38.4	9.3	12.5	0.0	62.0	27.0	4.0	7.0
3	26.8	0.6	16.4	10.3	0.0	1.1	6.2	0.0	/	/	/	/
4	38.9	0.9	16.9	8.0	6.7	0.0	0.0	17.8	/	/	/	/
5	38.1	2.6	43.6	0.0	0.0	0.0	0.0	16.2	65.0	13.0	6.0	16.0
6	/	/	/	/	/	/	/	/	/	/	/	/
7	40.1	1.0	19.1	8.0	3.3	2.2	1.9	24.4	61.0	18.0	10.0	11.0
8	25.7	0.6	3.8	0.0	14.7	1.5	10.1	0.0	65.0	24.0	8.0	3.0
9	16.4	2.4	24.5	3.4	33.2	0.0	6.0	0.0	66.0	30.0	2.0	2.0
10	30.9	0.8	33.2	15.4	17.5	1.5	0.0	0.0	15.0	41.0	43.0	1.0
11	37.6	4.1	17.2	11.4	14.1	1.7	0.0	0.0	20.0	44.0	35.0	1.0

4.2 Pore structure characteristics

A wide variety types of storage spaces were developed on the diabase, (e.g., primary storage spaces and secondary storage spaces).

The primary reservoir space covered a variety of pores and fractures formed during the magma cooling and diagenesis process, mainly processes (e.g., condensation shrinkage fractures (**Fig. 4a**) and intercrystal shrinkage microfractures (**Fig. 4b**). In general, the intercrystalline fractures developed in the hornfels were usually directional, straight, and discontinuous (**Fig. 4c**). Tectonic fractures developed in groups and were well filled with organic matter (**Fig. 4c**). The secondary storage space was primarily the storage space formed by external forces (e.g., tectonic action, hydrothermal alteration, weathering and leaching after the cooling of magma, which comprised various dissolution pores and fractures, structural cracks and so forth.

The minerals (e.g., feldspar) were altered and dissolved in the presence of hydrothermal fluids, thus leading to the formation of dissolution pores (**Fig. 4d**). Organic matter receives hydrothermal action to considerable a large number of organic matter pores (**Fig. 4e**). Minerals in slate form interlayer fractures (**Fig. 4f**). The pores in lacustrine shale are mainly inorganic mineral pores dominated by clay mineral pores. Clay mineral pores range from nanometer to micron with good connectivity, which provide space for the storage and flow of the shale oil (**Fig. 4g, h, i**). The none metamorphic shale also develops inorganic pores (e.g., intercrystal pores and chip hole).

Fig. 4. Pore types of the diabase and influenced shale from Cores, thin sections and FE-SEM images

Well, Z1, 1571.87 m, hornfuls, primary pore and condensation fractures (a), Well, Z1, 1580.78 m, shrinkage crack (b), Well, Z1, 1580.78 m, hornfuls, fractures filled with organic matter (c), Well, Z1 , 1657.65 m, gray-black layered slate, dissolved pores (d), Well, Z1, 1657.65 m, OM and organic pores (e), Well, Z1, 1664.82 m, chlorite in interlayer (f), Well, Z1, 1778.73 m, shale, structural fractures filled with calcite (g), Well, Z1, 1790.18 m, shale, chip hole filled with mica (h), Well, Z1, 1790.18 m,

shale, intercrystal pore (i).

According to the nitrogen adsorption and desorption curve types, the pore morphology characteristics can be inferred, and the different adsorption-desorption shape types reflect certain pore structure characteristics and types.

Fig. 5 presents the N_2 adsorption and desorption isotherms of the shale samples from the diabase metamorphic zone. The amount of N_2 adsorbed gradually increases with the increase of pressure until the relative pressure is close to 1, the saturated adsorption phenomenon will not appear, which indicates that there are large pores in the two groups of the shale. By analyzing the corresponding correlation between the shape of the adsorption ring and the shape of the pore, it is found that the pore structure of the zones affected by the diabase to different degrees has significant differences.

According to the IUPAC, the pores of adsorption hysteresis is divided into cylinder pores(H1), spherical pores(H2), lamellar, slit-wedge, shape pores(H3) narrow slit-like pores(H4) (Guan et al., 2020), the samples of low-grade metamorphic zone exhibited H3 hysteresis characteristics, while the samples of none metamorphic zone, high-grade metamorphic zone and intrusive zone exhibited H4 hysteresis loop characteristics, thus suggesting the pores in this area are mainly nanopores with a certain degree of irregularity. The rock was dominated by slab pores, while the intrusive zone and metamorphic zone were dominated by slit pores. **Table 3** lists the pore structure parameters calculated by N_2 adsorption. The specific surface area of the sample ranged from 2.958–16.400 m^2/g, with an average value of 7.45 m^2/g; the pore volume was 0.008–0.03 $mL \cdot g^{-1}$, with an average value of 0.017 $mL \cdot g^{-1}$, and the average pore size range was 2.897–4.152 nm. The average value was 3.42 nm; the specific surface area from the samples of high-grade metamorphic, low-grade metamorphic and none metamorphic zone shows tended to first increase, then decrease and then subsequently increase.

Fig. 5. N_2 adsorption isotherms curves of samples, Funing Formation, Subei Basin

Table.3. Organic geochemical parameters and pore parameters of samples, Funing Formation, Subei Basin

Sample	TOC /%	S_1 /(mg·g^{-1})	S_2 /(mg·g^{-1})	T_{max} /	*Ro* /%	Surface area / m²·g^{-1}	Pore volume / mL·g^{-1}	Oil contents /(μL·g^{-1})
1	0.98	0.11	0.17	402	2.20	5.08	0.014	0.050
2	1.30	0.28	0.27	409	2.17	5.11	0.013	0.032
3	0.06	0.01	0.01	414	/	/	/	/
4	0.05	0.01	0.01	440	/	/	/	
5	0.07	0.01	0.01	435	/	2.96	0.008	0.018
6	0.05	0.01	0.01	438	/	/	/	
7	0.04	0.01	0.01	423	/	/	/	0.021
8	2.04	0.61	0.23	408	1.35			
9	1.79	0.52	1.96	408	1.27	16.40	0.030	0.102
10	1.33	0.29	0.96	378	0.52	14.95	0.023	0.091
11	1.10	0.44	0.62	356	0.53	7.69	0.020	/

4.3 Oiliness distribution characteristics

The 2-D nuclear magnetic resonance analysis test is as shown in the figure below, where the horizontal and vertical coordinates are the T_1 and T_2 signal response sizes, respectively (Javed et al., 2019; Li et al., 2020a). Combining with the division of substances represented by different signal regions, **Fig. 6** illustrates the division of signal regions of different hydrogen-containing compound regions in the 2-D spectrum of the shale samples. The oil content applied in this study was mainly the sum of free oil and adsorbed oil, to obtain the relative oil content.

Fig. 6. Locations of each hydrogen-bearing components of shale on T_1-T_2 map of NMR tests.

The results of the 2D NMR experiment are presented in **Table 4** and **Fig. 7**, thus suggesting the oil content of this sample ranged from 0.08 to 1.39 $\mu L \cdot g^{-1}$, and the average content was 0.49 $\mu L \cdot g^{-1}$. As depicted in the table of classification results of various hydrides, the hydrides were mainly water, followed by hydrocarbons. The oil content distribution suggested that samples 1 and 3 of high-grade metamorphic zone achieved an average oil content of 0.0410 $\mu L \cdot g^{-1}$, samples 5 and 7 were diabase with an average oil content of 0.0195 $\mu L \cdot g^{-1}$, sample 9 of low-grade metamorphic zone oil content was 0.102 $\mu L \cdot g^{-1}$, sample 10 of none metamorphic zone achieved the shale oil content of 0.0910 $\mu L \cdot g^{-1}$; Moreover, the oil content increased and then decreased with the increase of the influence degree of diabase.

Table 4. Results of oiliness detected by high frequency 2D NMR map of samples, Funing Formation, Subei Basin

Sample	Quality /g	Total hydrocarbon content /μL	Structural water /$\mu L \cdot g^{-1}$	Free water /$\mu L \cdot g^{-1}$	Oil contents /$\mu L \cdot g^{-1}$	Free oil /$\mu L \cdot g^{-1}$	Adsorbed oil /$\mu L \cdot g^{-1}$
1	34.5	1492.5	2.000	41.200	0.050	0.012	0.038
2	35.8	1379.2	0.300	38.100	0.032	0.025	0.007

5	37.2	356.7	0.100	9.500	0.018	0.010	0.008
7	29.5	185.3	0.000	6.200	0.021	0.013	0.008
9	34.2	3004.9	0.000	87.700	0.102	0.020	0.082
10	20.9	2922.8	18.800	120.300	0.091	0.008	0.083

Fig. 7. 2D map from NMR tests of each phase of shale sample from Funing Formation, Subei basin

5 Discussion

5.1 The division zone of the intrusive-metamorphic reservoir

Since the lacustrine shale are affected by diabase to varying degrees, the degree of effect of diabase intrusion is divided into three zones (including the high-grade metamorphic zone, the low-grade metamorphic zone and the none metamorphic zone) in accordance with the electrical properties, lithology, hydrocarbon generation quality, and reservoir quality characteristics.

5.1.1 High-grade metamorphic zone

The study area mainly developed high-grade metamorphic belts and low-grade metamorphic zone. To be specific, the intermediate metamorphic zone is mainly horn rock, which is generally less than 12 m and has a horn rock structure. The main minerals are andalusite, cordierite, garnet, diopside, hematite, magnetite, etc.

The high-grade metamorphic zone mainly develops hornfels, which is mainly composed of clay (7.4–26.8%), quartz (0.6–17.5%), feldspar (0.0–16.4%) and carbonate (10.3–41.9%), with a typical blastic texture and chloritization occurred. High-grade metamorphic zone in this area has obvious logging response characteristics (**Fig. 8**). It has two low value and two high value, that is, low natural gamma, low sonic jet lag, high spontaneous potential and high resistivity.

The quality of hydrocarbon generation in the high-grade metamorphic zone is generally poor. The average values of TOC, S_1 and *Ro* are 0.78%, 0.13 $mg \cdot g^{-1}$ and 2.19%, respectively (**Fig. 9**). The degree of thermal evolution is high, but the abundance of organic matter is low, thus suggesting that the intrusion is intrusive. The area has low hydrocarbon generation potential.

The physical properties of the high-grade metamorphic zone are low-porosity-low-permeability and ultra-low permeability reservoirs. The marginal zone is

dominated by condensation shrinkage fractures and structural fractures, resulting in relatively poor physical properties in the high-grade metamorphic zone.

The pore structure parameters of the high-grade metamorphic zone are shown in **Table 3**. The average pore specific surface area, total pore volume and pore radius of the diabase samples are 5.10 $m^2 \cdot g^{-1}$, 0.0135 $mL \cdot g^{-1}$ and 3.033 nm, respectively. The pore structure of the sample is H4 type, thus suggesting that the pore morphology is slit pores, which is relatively poor.

Fig. 8. Characteristics of logging curves for lithology of diabase intrusion in Gaoyou sag, Subei Basin

5.1.2 Low-grade metamorphic zone

The low-metamorphic zone is located between the low-grade metamorphic zone. Moreover, the none metamorphic zone, and its logging response is characterized by transitional characteristics.

On conventional logging data, it shows the characteristics of five middle chrematistics: middle resistivity, middle sonic jet lag, middle spontaneous potential and neutron porosity and natural gamma (**Fig. 8**).

Slate largely develops in the low-metamorphic zone, which is relatively far away from the intrusive diabase. It is the least affected by the intrusion exhibits low metamorphism, and basically retains the original rock characteristics (e.g., the original mineral composition, argillaceous structure, and residual bedding). Slate lithology is dense, gray-black, with micro-fractures, which can be filled with calcite, mainly composed of clay (16.4–25.7%), quartz (0.6–2.4%), feldspar (3.8–24.5%) and carbonate (11.3–36.6%), identified under a microscope, the slate in the low-level metamorphic zone generally has a variable argillaceous structure or a variable silt argillaceous structure.

In general, the quality of hydrocarbon generation in the low-grade metamorphic zone is good. The average values of TOC, S_1 and Ro are 1.92%, 0.57 $mg \cdot g^{-1}$ and 1.31%,

respectively. The area exhibits good hydrocarbon generation potential (**Fig. 9**).

The physical properties of the metamorphic zone are low-porosity-low-permeability and ultra-low permeability reservoirs. The metamorphic zone is dominated by dissolved fractures, organic pore and interlayer fractures, thus causing relatively worse physical properties in the metamorphic zone.

Table 3 lists the pore structure parameters of the diabase intrusion area. The average pore specific surface area, total pore volume and pore radius of the diabase samples are 15.68 $m^2 \cdot g^{-1}$, 0.025 $mL \cdot g^{-1}$ and 3.969 nm, respectively. The pore structure of the sample is H3 type, thus suggesting that the pore morphology is slit pores, which is relatively good.

5.1.3 None metamorphic zone

The normal rock belt is mainly composed of lacustrine sedimentary gray-black mud shale, which has a wide variety of mineral components and strong vertical heterogeneity.

Its mineral composition mainly includes clay (30.9–37.6%), quartz (0.8–4.1%), feldspar (17.2–33.2%) and carbonate (25.5–32.9%), accompanied by a small amount of gypsum salt and pyrite, etc. The clay minerals are mainly composed of the illite-smectite layer and illite.

In conventional logging data, there are one high and two lows: high natural gamma, low sonic jet lag and low resistivity (**Fig. 8**). The quality of hydrocarbon generation in the metamorphic zone is generally poor. The average values of TOC, S_1 and *Ro* are 1.21%, 0.37 $mg \cdot g^{-1}$ and 0.53%, respectively (**Fig. 9**). The area exhibits better hydrocarbon generation potential than high-grade metamorphic zone. The physical properties of the none-metamorphic zone are low-porosity-low-permeability and ultra-low permeability reservoirs. The metamorphic zone is dominated by structural fractures, chip hole and intercrystal pores, such that relatively good physical properties are acheived in the normal zone. The pore structure parameters of the normal area are shown in **Table 3**. The average pore specific surface area, total pore volume and pore

radius of the diabase samples are 7.69 $m^2 \cdot g^{-1}$, 0.023 $mL \cdot g^{-1}$ and 2.99 nm, respectively. The pore structure of the sample is H3 type, thus suggesting the pore morphology is slit pores, which is relatively better than high-grade metamorphic zone (**Fig. 9**).

Fig. 9. Characteristics of diabase, metamorphic reservoir and normal zone in Gaoyou Sag

5.2 The distribution characteristics of oiliness

The lacustrine shale of the Funing Formation is an organic-rich shale, affected by diabase to different degrees; it exhibits significant oil-bearing heterogeneity. The predecessors have commonly employed free hydrocarbon S_1 and oil content to characterize the oil content.

The samples of diabase, with an average of S_1 achieved the oil content of 0.01 $mg \cdot g^{-1}$ and 0.020 $\mu L \cdot g^{-1}$. The sample of high-grade metamorphic zone with an average of S_1, oil contents are 0.20 $mg \cdot g^{-1}$ and 0.041 $\mu L \cdot g^{-1}$. The sample of low-grade metamorphic zone with an average of achieved the oil content of 0.57 $mg \cdot g^{-1}$ and 0.102 $\mu L \cdot g^{-1}$. The sample of none metamorphic zone with an average of S_1, oil contents are 0.37 $mg \cdot g^{-1}$ and 0.091 $\mu L \cdot g^{-1}$(**Fig. 10**).

Fig. 10. Distribution of S_1 (a) and oil contents (b) in diabase, metamorphic and normal zone in Gaoyou Sag

According to the results of oil content in different zones, the oil content is the highest in low-grade metamorphic zone, and the none metamorphic zone gets worse but the high-grade metamorphic zone achieves the least oil content. The oil content of lacustrine organic-rich shale tends to decrease.

The microscopic oiliness of continental shale is affected by the reservoir space system and mineral wettability. The degree of effect of diabase is different, and its storage space system and mineral type are quite different, and its oiliness is also affected. It can be seen that the shale affected by the diabase in the second member of the Funing formation contains oil as a whole, but the oil enrichment space and mineral type are quite different. The edges of mineral particles (e.g., pyroxene and feldspar) in the high-grade metamorphic zone emit scattered dark blue or bright blue fluorescence (**Fig. 11**), and the fluorescence display is poor. It is because the diabase has no hydrocarbon-generated ability, and the oil mainly comes from migration, such that the overall oil-

bearing property is extremely poor. Minerals and organic matter in the low metamorphic zone exhibit scattered blue fluorescence features (**Fig. 11**), and dark fluorescence features in microfractures are significant. Organic pores are generated under the effect of diabase intrusion heat, thus laying a spatial basis for oil reservoirs. In general, even the smallest organic pores in shale oil reservoirs are oil-bearing for their lipophilicity, consistent with the 2D NMR characterization. Relatively good results for oiliness are corresponding (**Fig. 11**). The edges of mineral particles in none metamorphic zone (e.g., feldspar and dolomite), are scattered with bright green fluorescence, and the intragranular pores formed by the dissolution of feldspar and lipophilic dolomite particles are characterized using scattered bright green fluorescence (**Fig. 11**), thus suggesting that inorganic pores (e.g., intergranular pores and dissolution pores) in unaffected shale are the main storage spaces for oil and gas.

Fig. 11. Fluorescence thin sections under plane polarized light, fluorescence light and 2D map of NMR to show oiliness distribution characteristics in different zones of Funing Formation in Subei Basin.

5.3 Distribution modes of oiliness affected by diabase

Diabase intrusion and normal surrounding rock contact resulted in the intrusion-metamorphic-normal surrounding rock complex area. The oil-bearing property varied significantly with the different degrees of diabase intrusion, and the differences were largely indicated as follows (**Fig. 12**).

High-grade metamorphic zone: hornfels refers to a high-grade metamorphic rock. The volatile components in the magma tend to separate, accumulate, and expand from the magma with the invasion of magma and reduction of the pressure. Subsequently, the components are carried by the magma upward as liquid and gas and gathered in the fringe zone. In the process of magma cooling, condensation shrinks due to volume changes, forming considerable condensation shrinkage joints. It provides space for oil and gas reservoirs, but due to decarbonization, the ability to generate hydrocarbons is completely lost. The oil and gas are mainly derived from exogenous hydrocarbons and have the worst oil-bearing properties.

Low-grade metamorphic zone: with the intrusion and condensation of magma, in addition to the high salinity fluid released by the magma itself, the surrounding rocks in the metamorphic zone undergo dehydration and decarbonization, and an average of 2 mol fluids are released per kilogram of the shale (Liu et al., 2016). These are the instantaneous hydrothermal fluids. It is discharged to the surrounding rock to form a circulation or one-way flow to exchange heat and material with the outside world. During this process, considerable dissolution pores and cracks are produced, and the storage properties are better than low-grade metamorphic zone. It also increases the local formation temperature in the basin, thereby reducing the hydrocarbon generation threshold depth of lacustrine shale organic matter and accelerating the conversion of organic matter to oil and gas. Thus, the low-grade metamorphic zone achieves the most oil content.

None metamorphic zone: it is normal mudstone not affected by diabase intrusion. At this stage, mudstone undergoes normal diagenesis. With the increase of the burial

depth, the degree of the thermal evolution of organic matter tends to increase to produce oil and gas, and a small number of matrix pores develop. It has not been affected by the intrusion of diabase, and it has just entered the oil generation threshold, with less oil generation. Accordingly, the oil content is more than that of high-grade metamorphic zone but less than that of the low-grade metamorphic zone.

The oil enrichment mode of lacustrine shale by diabase intrusion was built in accordance with the comprehensive research of the petrology, hydrocarbon generation, reservoir characteristics and oiliness of contact metamorphic mudstone. After diabase intrudes into lacustrine shale, the shale can be divided into the normal shale belt, the low-level metamorphic zone and the advanced metamorphic zone with the increase of intrusion distance and metamorphism. First, with the increase of metamorphism, the degree of thermal evolution of organic matter increases. The major reason for this finding is that magma intrusion carries considerable heat to heat the formation water, due to the heat propagation caused by the local ground temperature of the basin to rise, thus reducing the throttle limit depth and facilitating the organic matter hydrocarbon generation. Second, the specific surface area and total pore volume of the shale in the low metamorphic zone are better than those of normal shale, whereas the pore structure parameters of the reservoir in the high metamorphic zone are worse. Lastly, the oil content of different metamorphic zones exhibits significant heterogeneity. The low metamorphic zone exhibits a higher oil content than the normal shale, whereas the high metamorphic zone achieves the least oil content. Accordingly, this model takes on a critical significance in expanding the field of oil and gas exploration for in-depth understanding and exploration of the effect of diabase intrusion on shale oil enrichment.

Fig. 12. Distribution modes of oiliness influenced by diabase

6 Conclusions

(1) The lacustrine shale in the Funing formation is metamorphosed due to diabase intrusion. The zone affected by diabase intrusion is divided into the none metamorphic zone, the low-grade metamorphic zone, the high-grade metamorphic zone and intrusive with the increase of the metamorphic degree. The shale is altered into slate and hornfels that are characterized by chloritization of clay matrices. The higher the degree of metamorphism, the more chlorite content will be.

(2) The metamorphic rocks are altered as hydrocarbon reservoirs after diabase intrusion in the study area. Compared with the none metamorphic zone, the low-grade metamorphic zone shale exhibited more favorable reservoir properties, whereas the high-grade metamorphic zone exhibits worse reservoir properties in the metamorphic zone.

(3) S_1 and 2D NMR exhibited significant heterogeneity of oil content in different metamorphic zones. The oil content of low-grade metamorphic zone is higher than those of none metamorphic zone. However, the oil content of high-grade metamorphic zone is the least. S_1 and oil content shows good correlations with chlorites content. After the diabase intrudes into the lacustrine shale, the oil content of the low metamorphic zone becomes better, whereas the high metamorphic zone becomes worse.

(4) A distribution model of oiliness affected by diabase intrusion is established. Upper metamorphic zone is thicker than lower metamorphic zone due to diabase intrusion. Diabase intrusion has caused obvious heterogeneity of hydrocarbon generation quality and reservoir quality in different zones.

Declaration of competing interest

The authors declare that they have no known competing financial interests or personal relationships that could have appeared to influence the work reported in this paper.

Acknowledgments

This work was financially supported by the National Natural Science Foundation of China (Grant No. 42072150). We also thank SINOPEC Jiangsu Oilfield Company for providing samples and data access.

References

Aljamaan, H., Al Ismail, M., Kovscek, A.R., 2017. Experimental investigation and Grand Canonical Monte Carlo simulation of gas shale adsorption from the macro to the nano scale. Journal of Natural Gas Science and Engineering 48, 119–137. https://doi.org/10.1016/j.jngse.2016.12.024

Annuar, A.S., Rahman, R.A., Munir, A., Murad, A., El-enshasy, H.A., Illias, R., 2021. Analysis of micropore size distribution using Dubinin's theory of volume filling - Effect of particle size on pore characterization of organic-rich Indian shales. Carbohydrate Polymers 118-159. https://doi.org/10.1016/j.jngse.2022.104746

Chen, S., Yao, S., Wang, Y., Liu, S., Wang, X., Zhang, Y., Wang, H., 2021. Investigation of pore evolution and variation with magma intrusion on Permian Gufeng shale formation and their implications on gas enrichment. Journal of Natural Gas Science and Engineering 96, 104277. https://doi.org/10.1016/j.jngse.2021.104277

Cheng, Q., Zhang, M., Li, H., 2019. Anomalous distribution of steranes in deep lacustrine facies low maturity-maturity source rocks and oil of Funing formation in Subei Basin. Journal of Petroleum Science and Engineering 181, 1061-90. https://doi.org/10.1016/j.petrol.2019.106190

Cid, H.E., Carrasco-Núñez, G., Manea, V.C., Vega, S., Castaño, V., 2021. The role of microporosity on the permeability of volcanic-hosted geothermal reservoirs: A case study from Los Humeros, Mexico. Geothermics 90. https://doi.org/10.1016/j.geothermics.2020.102020

de Souza, Z.S., Wang, C., Jin, Z.M., Li, J.W., Yang, J., Botelho, N.F., Viana, R.R., dos Santos, L., Liu, P.L., Li, W., 2019. Pyrometamorphic aureoles of Cretaceous sandstones and shales by Cenozoic basic intrusions, NE Brazil: Petrograhic, textural, chemical and experimental approaches. Lithos 326–327, 90–109. https://doi.org/10.1016/j.lithos.2018.11.033

Du, H.Y., Chen, J.F., Ma, X., Han, B.F., Liu, B., Simon, A., Liu, J.L., Ren, R., Li, C., Zhou, L.M., Lei, Z.L., 2019. Origin and tectonic significance of the Hoboksar ophiolitic mélange in northern West Junggar (NW China). Lithos 336–337, 293–309. https://doi.org/10.1016/j.lithos.2019.04.010

Gao, G., Yang, S., Zhang, W., Wang, Y., Gang, W., Lou, G., 2018. Organic geochemistry of the lacustrine shales from the Cretaceous Taizhou Formation in the Gaoyou Sag, Northern Jiangsu Basin. Marine and Petroleum Geology 89, 594–603. https://doi.org/10.1016/j.marpetgeo.2017.10.023

Goodarzi, F., Gentzis, T., Dewing, K., 2019. Influence of igneous intrusions on the thermal maturity of organic matter in the Sverdrup Basin, Arctic Canada. International Journal of Coal Geology 213, 103280. https://doi.org/10.1016/j.coal.2019.103280

Guan, M., Liu, X., Jin, Z., Lai, J., 2020. The heterogeneity of pore structure in lacustrine shales: Insights from multifractal analysis using N_2 adsorption and mercury intrusion. Marine and Petroleum Geology 114, 104150.

https://doi.org/10.1016/j.marpetgeo.2019.104150

Hormozzade, F., Craven, J.A., Motazedian, D., Grasby, S.E., Tschirhart, V., 2022. Geothermics Modeling a fractured geothermal reservoir using 3-D AMT data inversion : Insights from Garibaldi Volcanic Belt , British Columbia , Canada. Geothermics 105, 102528. https://doi.org/10.1016/j.geothermics.2022.102528

Javed, M.A., Komulainen, S., Daigle, H., Zhang, B., Vaara, J., Zhou, B., Telkki, V.V., 2019. Determination of pore structures and dynamics of fluids in hydrated cements and natural shales by various 1H and 129Xe NMR methods. Microporous and Mesoporous Materials 281, 66–74. https://doi.org/10.1016/j.micromeso.2019.02.034

Koltzer, N., Möller, P., Inbar, N., Siebert, C., Rosenthal, E., Magri, F., 2017. Thermal impacts of magmatic intrusions: A hypothesis of paleo-heating processes in the Tiberias Basin, Jordan-Dead Sea Transform. Energy Procedia 125, 80–87. https://doi.org/10.1016/j.egypro.2017.08.071

Li, J., Jiang, C., Wang, M., Lu, S.F., Chen, Z., Chen, G., Li, Jijun, Li, Z., Lu, S.D., 2020. Adsorbed and free hydrocarbons in unconventional shale reservoir: A new insight from NMR T1-T2 maps. Marine and Petroleum Geology 116, 104311. https://doi.org/10.1016/j.marpetgeo.2020.104311

Li, Y., Li, M., Zhang, J., Pang, Q., Zou, C., Shu, H., Wang, G., 2020. Influence of the Emeishan basalt eruption on shale gas enrichment: A case study of shale from Wufeng-Longmaxi formations in northern Yunnan and Guizhou provinces. Fuel 282. https://doi.org/10.1016/j.fuel.2020.118835

Liu, C., Gu, L., Wang, J., si, S., 2019. Reservoir characteristics and forming controls of intrusive-metamorphic reservoir complex: A case study on the diabase-metamudstone rocks in the Gaoyou sag, eastern China. Journal of Petroleum Science and Engineering 173, 705–714. https://doi.org/10.1016/j.petrol.2018.10.063

Liu, C., Xie, Q., Wang, G., Zhang, C., Wang, L., Qi, K., 2016. Reservoir properties and controlling factors of contact metamorphic zones of the diabase in the northern slope of the Gaoyou Sag, Subei Basin, eastern China. Journal of Natural Gas Science and Engineering 35, 392–411. https://doi.org/10.1016/j.jngse.2016.08.070

Liu, R., Luo, B., Li, Y., Qiu, N., Wang, W., Zhang, Y., He, Q., Pei, S., 2021. Relationship between Permian volcanic rocks distribution and karst paleogeomorphology of Maokou Formation and its significance for petroleum exploration in western Sichuan Basin, SW China. Petroleum Exploration and Development 48, 670–682. https://doi.org/10.1016/S1876-3804(21)60053-8

Liu, X., Jin, Z., Lai, J., Fan, X., Guan, M., Shu, H., Wang, G., Liu, M., Luo, Y., 2021. Fractal behaviors of NMR saturated and centrifugal T2 spectra in oil shale reservoirs: The Paleogene Funing formation in Subei basin, China. Marine and Petroleum Geology 129, 105069. https://doi.org/10.1016/j.marpetgeo.2021.105069

Ma, X., Li, G., Ying, D., Zhang, B., Li, Y., Dai, X., Fan, Y., Zeng, Y., 2019. Distribution and gas-bearing properties of Permian igneous rocks in Sichuan Basin,

SW China. Petroleum Exploration and Development 46, 228–237. https://doi.org/10.1016/S1876-3804(19)60004-2

Martins, C.M.S., Cerqueira, J.R., Ribeiro, H.J.P.S., Garcia, K.S., da Silva, N.N., Queiroz, A.F. de S., 2020. Evaluation of thermal effects of intrusive rocks on the kerogen present in the black shales of Irati Formation (Permian), Paraná Basin, Brazil. Journal of South American Earth Sciences 100, 102559. https://doi.org/10.1016/j.jsames.2020.102559

Othman, R., Arouri, K.R., Ward, C.R., McKirdy, D.M., 2001. Oil generation by igneous intrusions in the northern Gunnedah Basin, Australia, Organic Geochemistry.32, 1219-1232.. https://doi.org/10.1016/S0146-6380(01)00089-4

Rodriguez Monreal, F., Villar, H.J., Baudino, R., Delpino, D., Zencich, S., 2009. Modeling an atypical petroleum system: A case study of hydrocarbon generation, migration and accumulation related to igneous intrusions in the Neuquen Basin, Argentina. Marine and Petroleum Geology 26, 590–605. https://doi.org/10.1016/j.marpetgeo.2009.01.005

Rong, H., Jiao, Y., Wu, L., Zhao, X., Cao, M., Liu, W., 2021. Effects of igneous intrusions on diagenesis and reservoir quality of sandstone in the Songliao Basin, China. Marine and Petroleum Geology 127, 104980. https://doi.org/10.1016/j.marpetgeo.2021.104980

Ruz Ginouves, J., Gerbault, M., Cembrano, J., Iturrieta, P., Sáez Leiva, F., Novoa, C., Hassani, R., 2021. The interplay of a fault zone and a volcanic reservoir from 3D elasto-plastic models: Rheological conditions for mutual trigger based on a field case from the Andean Southern Volcanic Zone. Journal of Volcanology and Geothermal Research 418. https://doi.org/10.1016/j.jvolgeores.2021.107317

Shu, Y., Sang, S.X., Lin, Y.X., Zhou, X.Z., Wang, H., Wang, Z.L., 2021. The influence of magmatic-hydrothermal activities on porosity and permeability of sandstone reservoirs in the Linxing area, Ordos Basin, Northern China. Journal of Asian Earth Sciences 213, 104741. https://doi.org/10.1016/j.jseaes.2021.104741

Spacapan, J.B., Palma, J.O., Galland, O., Manceda, R., Rocha, E., D'Odorico, A., Leanza, H.A., 2018. Thermal impact of igneous sill-complexes on organic-rich formations and implications for petroleum systems: A case study in the northern Neuquén Basin, Argentina. Marine and Petroleum Geology 91, 519–531. https://doi.org/10.1016/j.marpetgeo.2018.01.018

Teixeira, C.A.S., Bello, R.M.S., Almeida, N.S., Pestilho, A., Brochsztain, S., de Queiroz, T.B., Andrade, L.S., Júnior, D.F.G., Sawakuchi, A.O., 2020. Hydrocarbon generation in the Permian Irati organic-rich shales under the influence of the early cretaceous Paraná Large Igneous Province. Marine and Petroleum Geology 117, 104410. https://doi.org/10.1016/j.marpetgeo.2020.104410

Thomaz Filho, A., Mizusaki, A.M.P., Antonioli, L., 2008. Magmatism and petroleum exploration in the Brazilian Paleozoic basins. Marine and Petroleum Geology 25, 143–151. https://doi.org/10.1016/j.marpetgeo.2007.07.006

Wu, L., Zhu, Y.M., Chen, S.B., Wang, H., 2011. Response of coal reservoir porosity to magma intrusion in the Shandong Qiwu Mine, China. Mining Science and

Technology 21, 185–190. https://doi.org/10.1016/j.mstc.2011.02.008

Xu, K., Yu, B., Gong, H., Ruan, Z., Pan, Y., Ren, Y., 2015. Carbonate reservoirs modified by magmatic intrusions in the Bachu area, Tarim Basin, NW China. Geoscience Frontiers 6, 779–790. https://doi.org/10.1016/j.gsf.2015.02.002

Ye, T., Chen, A., Niu, C., Wang, Q., Hou, M., 2022. Characteristics, controlling factors and petroleum geologic significance of fractures in the Archean crystalline basement rocks: A case study of the South Jinzhou oilfield in Liaodong Bay depression, North China. Journal of Petroleum Science and Engineering 208, 109504. https://doi.org/10.1016/j.petrol.2021.109504

Yu, B., Santosh, M., Wang, M.X., Yang, C.X., 2022. Paleoproterozoic emplacement and Cambrian ultrahigh-temperature metamorphism of a layered magmatic intrusion from the Central Madurai Block, southern India: From Columbia to Gondwana. Geoscience Frontiers 13, 101260. https://doi.org/10.1016/j.gsf.2021.101260

Yu, Z., Liu, K., Liu, L., Qu, X., Yu, M., Zhao, S., Ming, X., 2016. Characterization of Paleogene hydrothermal events and their effects on reservoir properties in the Qikou Sag, eastern China. Journal of Petroleum Science and Engineering 146, 1226–1241. https://doi.org/10.1016/j.petrol.2016.08.026

Zhang, Z., Yu, H., Chen, H., Du, S., Li, C., 2022. Quantitative characterization of fracture-pore distribution and effects on production capacity of weathered volcanic crust reservoirs: Insights from volcanic gas reservoirs of the Dixi area, Junggar Basin, Western China. Marine and Petroleum Geology 140, 105651. https://doi.org/10.1016/j.marpetgeo.2022.105651

Zou, C.N., Zhao, W.Z., Jia, C.Z., Zhu, R.K., Zhang, G.Y., Zhao, X., Yuan, X.J., 2008. Formation and distribution of volcanic hydrocarbon reservoirs in sedimentary basins of China. Petroleum Exploration and Development 35, 257–271. https://doi.org/10.1016/S1876-3804(08)60071-3

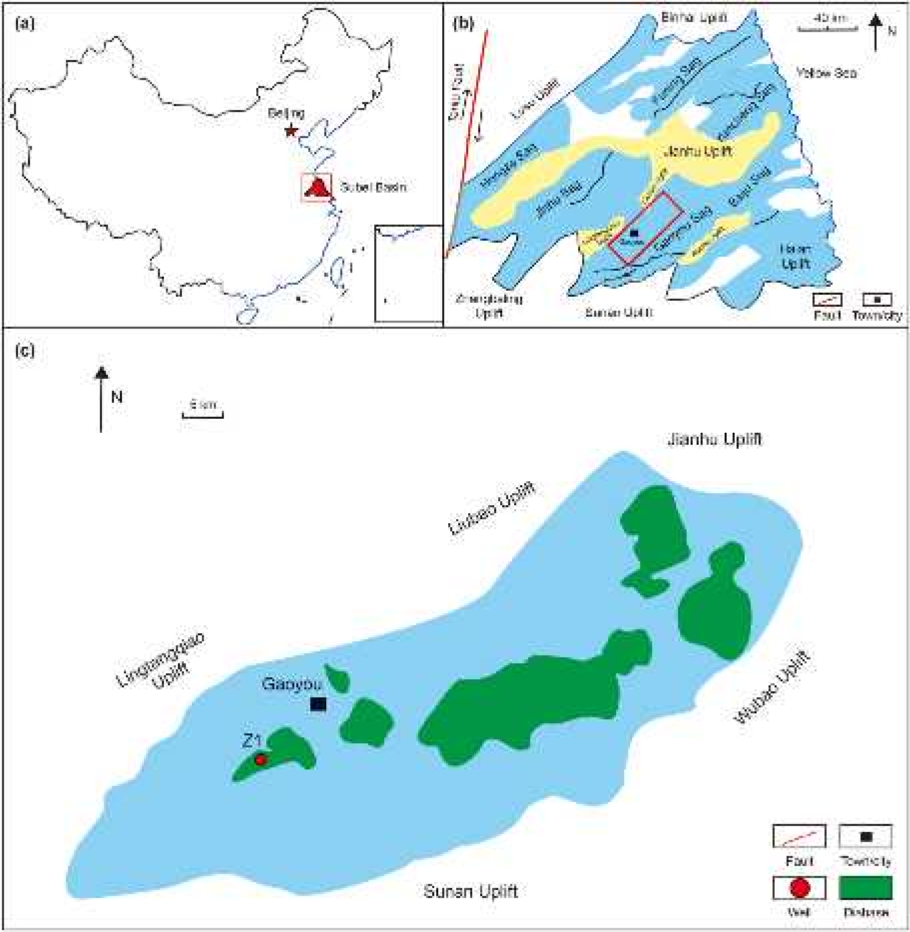

(a)
Beijing
Subei Basin
(b)
Binhai Uplift
N
Yellow Sea
Jianhu Uplift
Sunan Uplift
Fault
Town/city
(c)
N
5 km
Jianhu Uplift
Liubao Uplift
Lingtangqiao Uplift
Gaoyou
Wubao Uplift
Z1
Sunan Uplift
Fault
Town/city

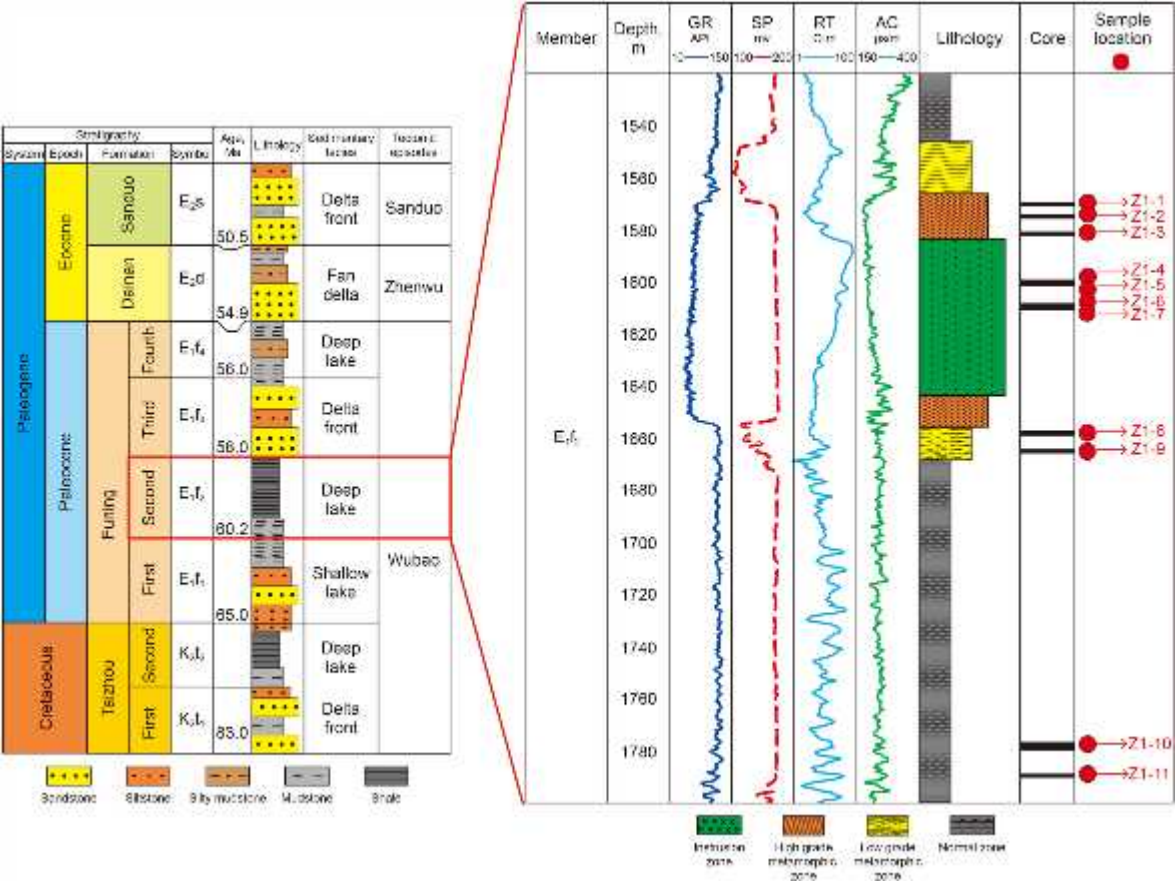
Stratigraphy
System
Epoch
Formation
Symbol
Age, Ma
Lithology
Sedimentary facies
Tectonic episodes
Paleogene
Eocene
Paleocene
Cretaceous
Sanduo
Deinan
Funing
Fourth
Third
Second
First
Taizhou
Second
First
E_2s
E_2d
E_1f_4
E_1f_3
E_1f_2
E_1f_1
K_2t_2
K_2t_1
50.5
54.9
56.0
56.0
60.2
65.0
83.0
Delta front
Fan delta
Deep lake
Delta front
Deep lake
Shallow lake
Deep lake
Delta front
Sanduo
Zhenwu
Wubao
Sandstone
Siltstone
Silty mudstone
Mudstone
Shale
Member
Depth m
GR API
SP mV
RT Ω·m
AC μs/m
Lithology
Core
Sample location
E_1f_1
1540
1560
1580
1600
1620
1640
1660
1680
1700
1720
1740
1760
1780
Z1-1
Z1-2
Z1-3
Z1-4
Z1-5
Z1-6
Z1-7
Z1-8
Z1-9
Z1-10
Z1-11
Instruction zone
High grade metamorphic zone
Low grade metamorphic zone
Normal zone

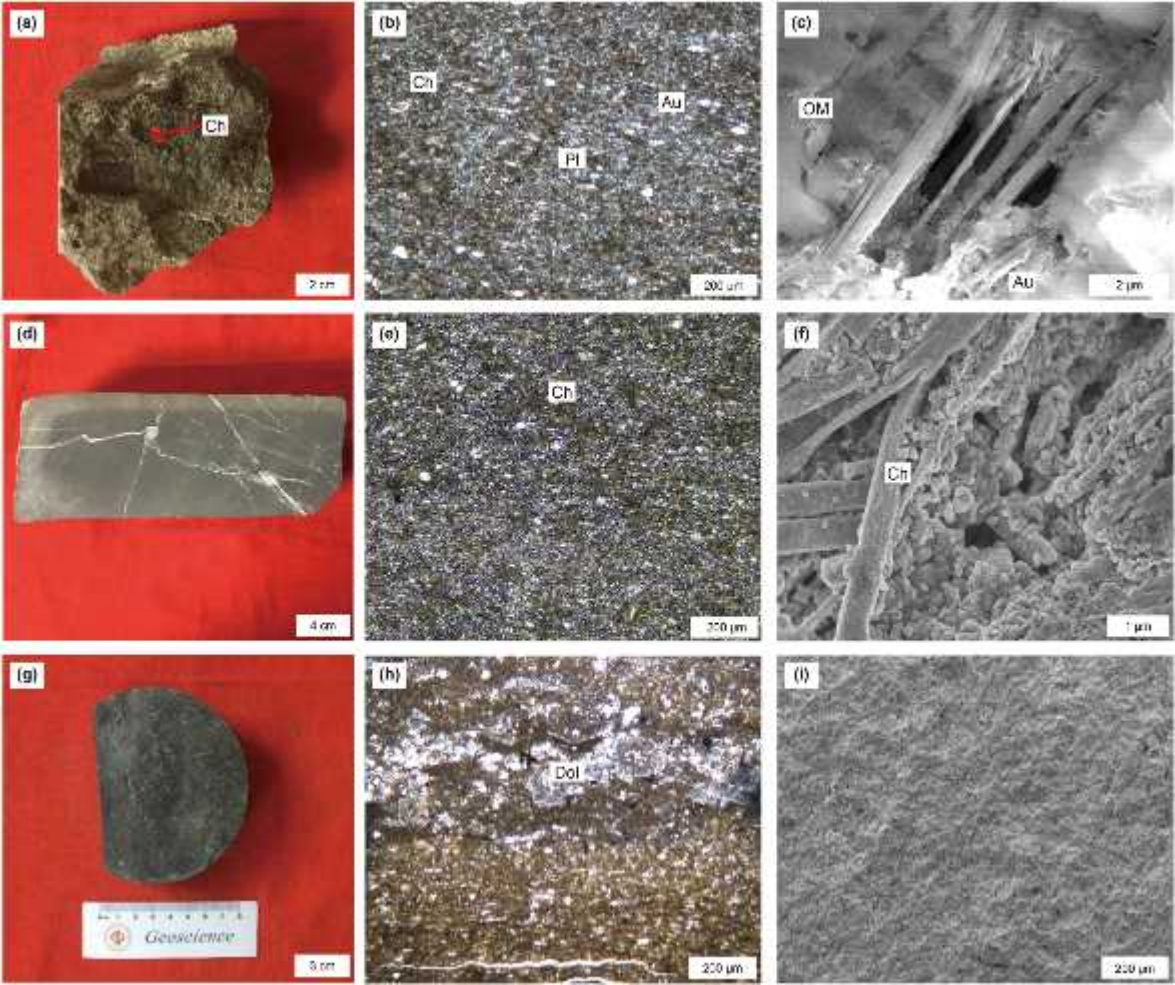
(a)
Ch
2 cm
(b)
Ch
Au
Pl
200 μm
(c)
OM
Au
2 μm
(d)
4 cm
(e)
Ch
200 μm
(f)
Ch
1 μm
(g)
Geoscience
5 cm
(h)
Dol
200 μm
(i)
200 μm

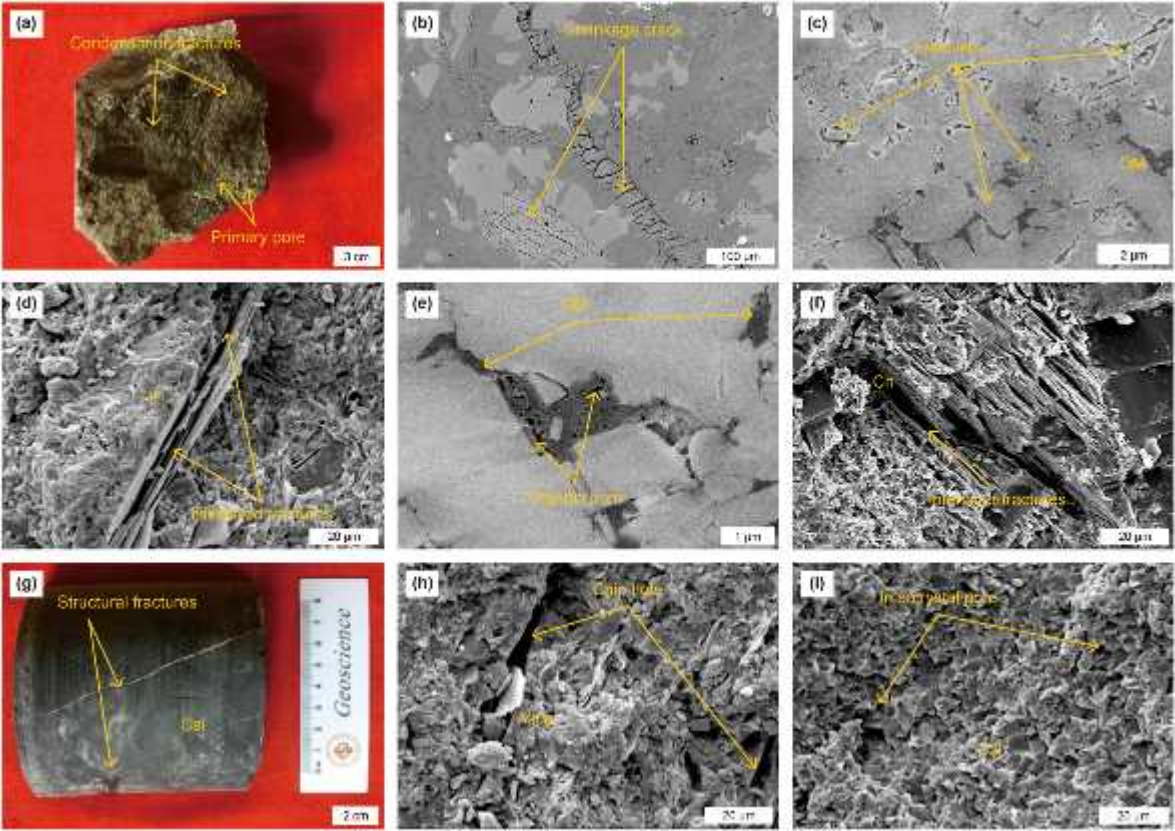
(a)
Condensation fractures
Primary pore
3 cm
(b)
Cleavage cracks
100 μm
(c)
Cleavage
Cal
2 μm
(d)
Cal
Interparticle fractures
20 μm
(e)
Cal
Cleavage cracks
1 μm
(f)
Cal
Interparticle fractures
20 μm
(g)
Structural fractures
Dol
Geoscience
2 cm
(h)
Cleavage
Dol
20 μm
(i)
Intercrystal pore
Dol
20 μm

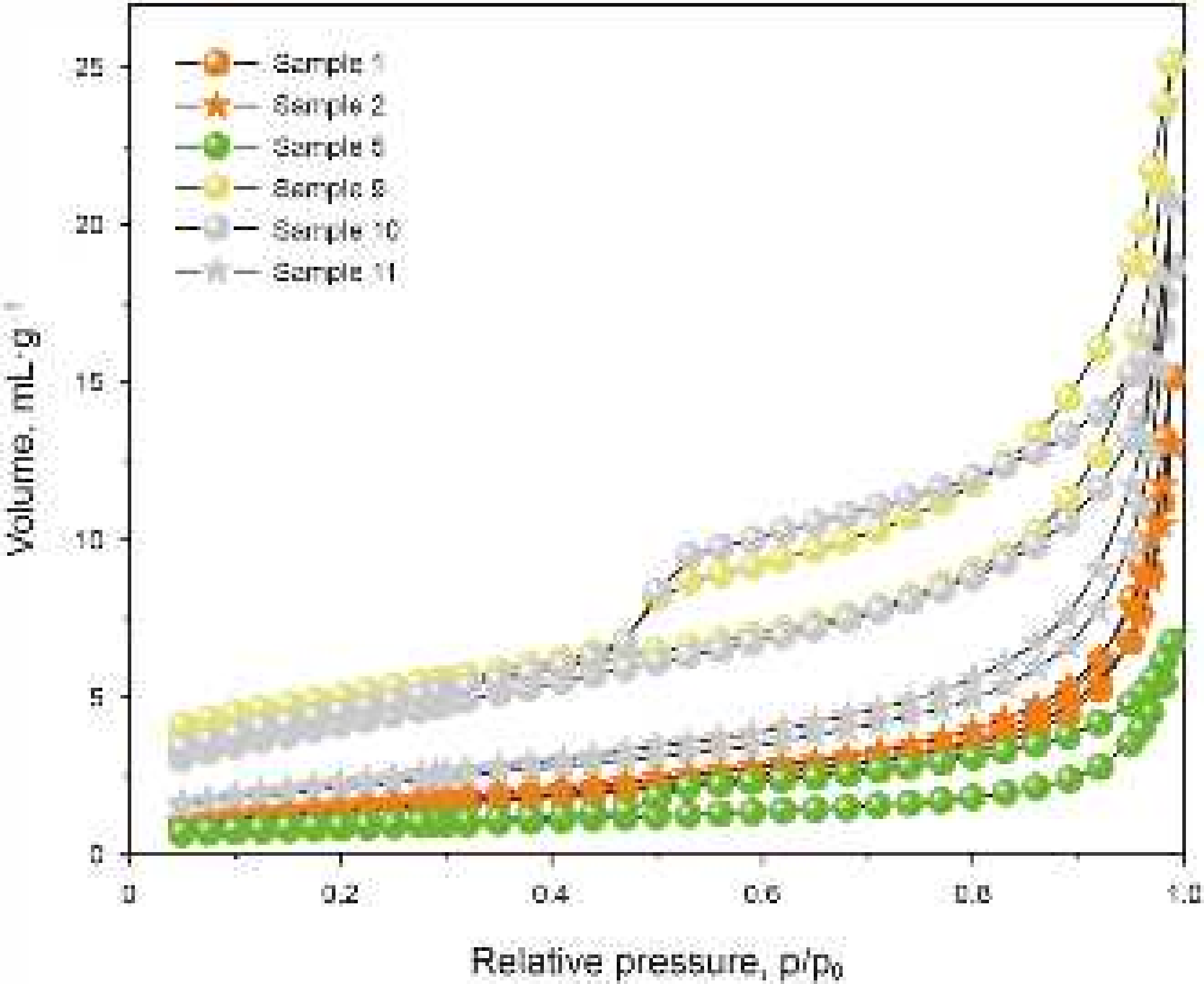
Sample 1
Sample 2
Sample 9
Sample 8
Sample 10
Sample 11
25
20
15
10
5
0
Volume, mL·g⁻¹
0
0.2
0.4
0.6
0.8
1.0
Relative pressure, p/p0

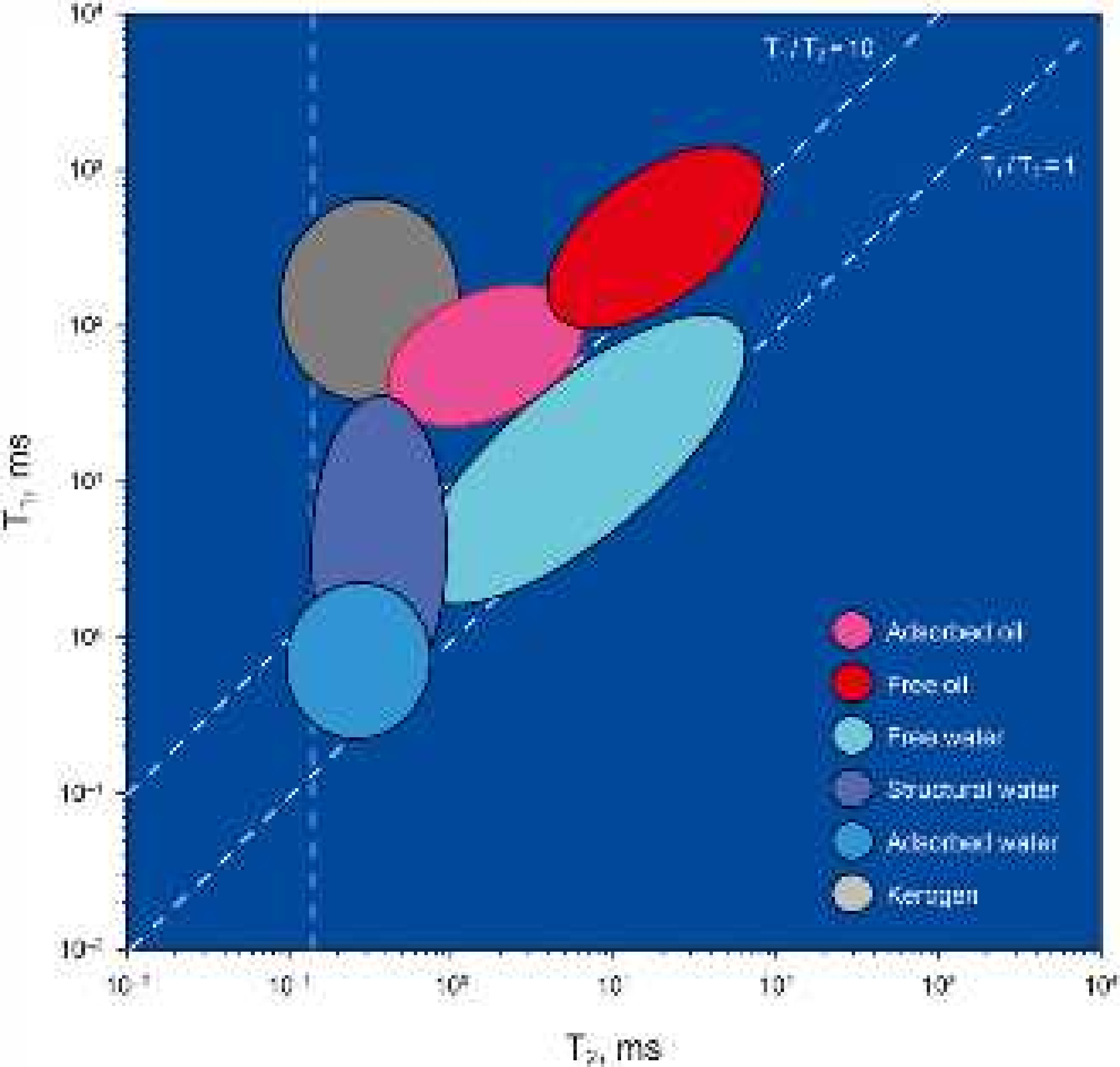
T1/T2=10
T1/T2=1
Adsorbed oil
Free oil
Free water
Structural water
Adsorbed water
Kerogen
T1, ms
T2, ms

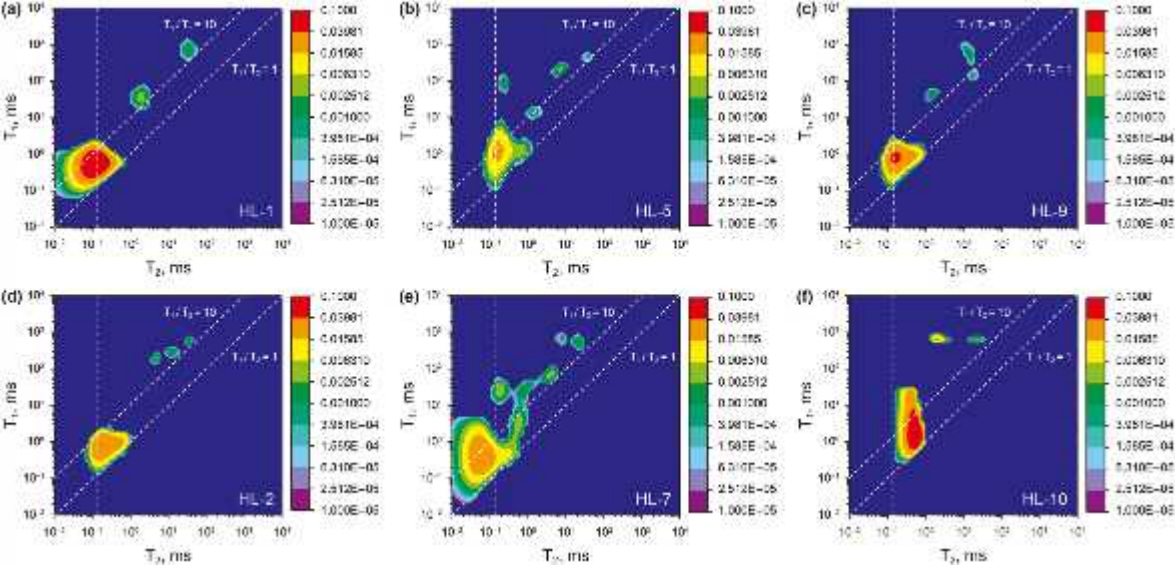
(a)
(b)
(c)
(d)
(e)
(f)
HL-1
HL-5
HL-9
HL-2
HL-7
HL-10
T1/T2=10
T1/T2=1
T1, ms
T2, ms

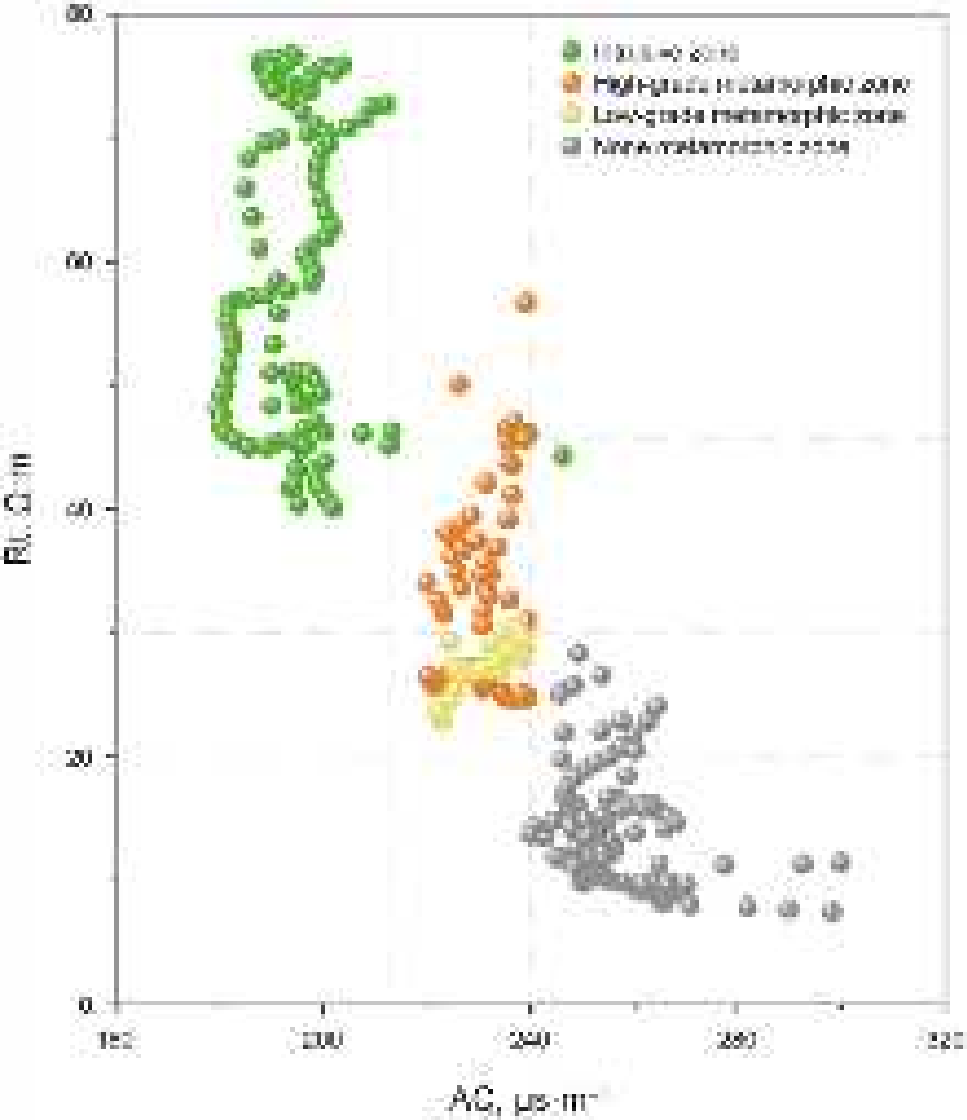
AC, μs·m⁻¹

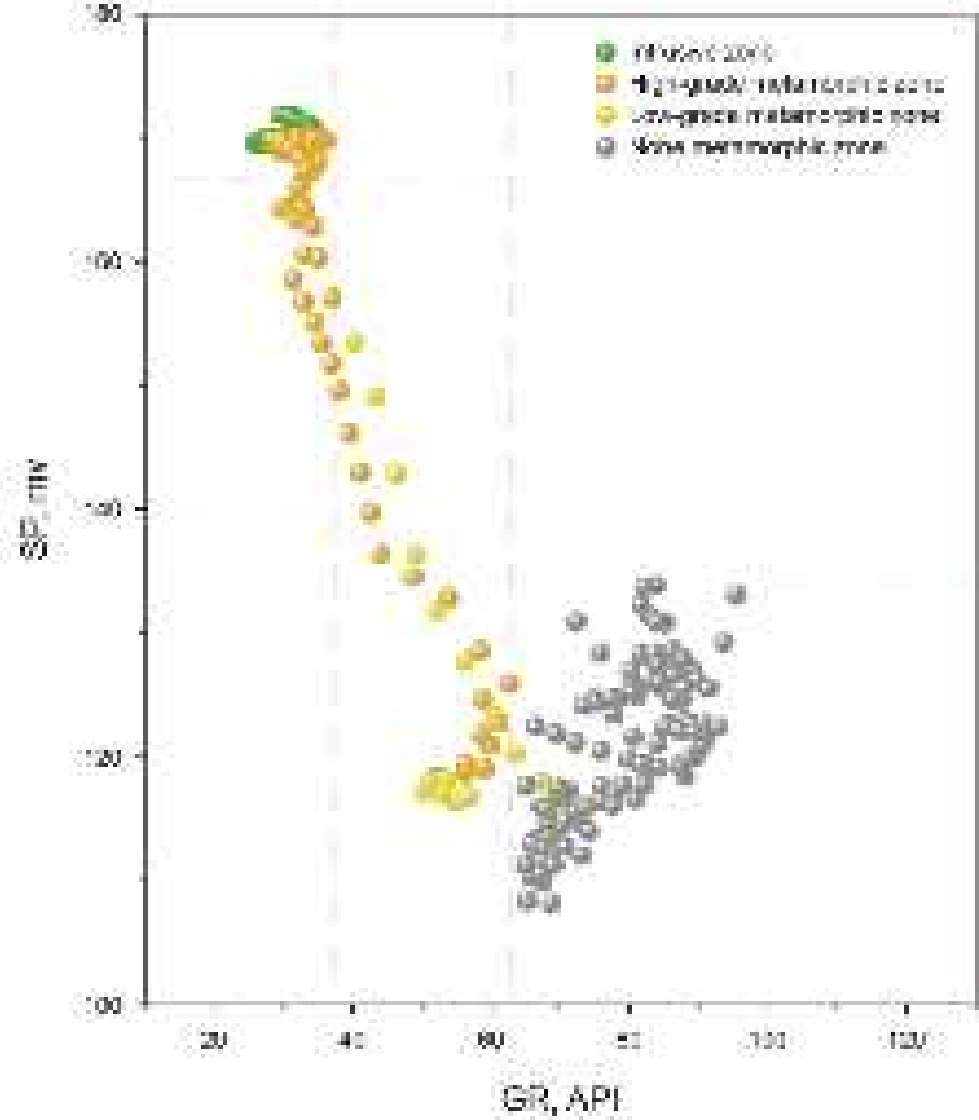
GR, API

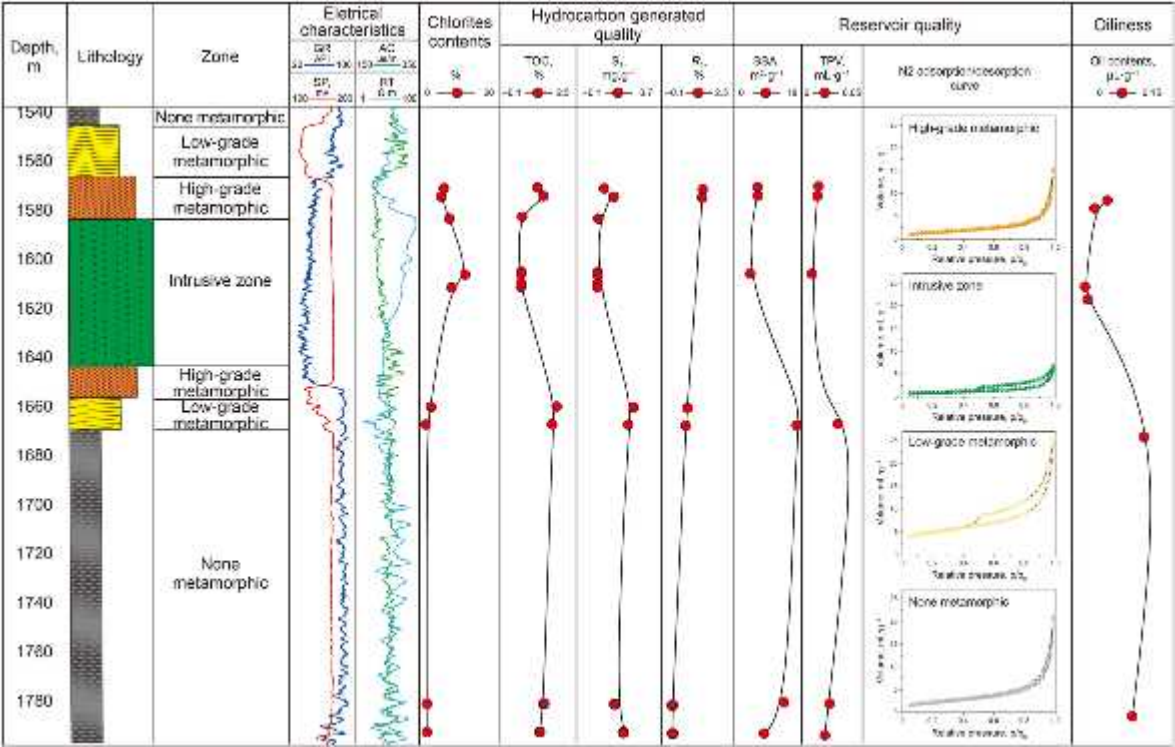
Depth, m
Lithology
Zone
Eletrical characteristics
Chlorites contents
Hydrocarbon generated quality
Reservoir quality
Oiliness
None metamorphic
Low-grade metamorphic
High-grade metamorphic
Intrusive zone
High-grade metamorphic
Low-grade metamorphic
None metamorphic
1540
1560
1580
1600
1620
1640
1660
1680
1700
1720
1740
1760
1780
%
TOC, %
S_1, mg/g
R_o, %
SSA, $m^2 \cdot g^{-1}$
TPV, $mL \cdot g^{-1}$
N2 adsorption/desorption curve
Oil contents, $\mu L \cdot g^{-1}$
Intrusive zone
Low-grade metamorphic
None metamorphic

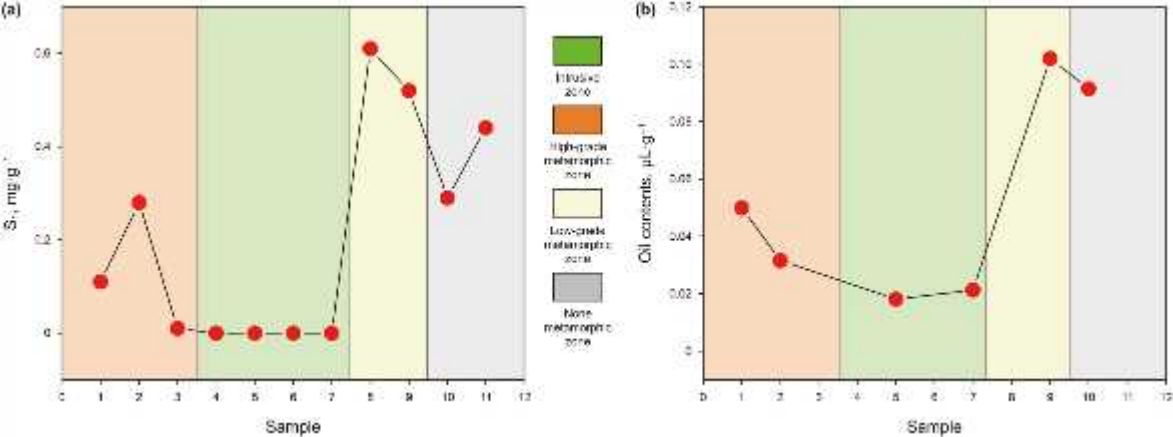
(a)
S1, mg·g⁻¹
0.6
0.4
0.2
0
0
1
2
3
4
5
6
7
8
9
10
11
12
Sample
Immature zone
High-grade mature oil zone
Low-grade mature oil zone
Mature zone
(b)
Oil contents, μL·g⁻¹
0.10
0.08
0.06
0.04
0.02
0
0
1
2
3
4
5
6
7
8
9
10
11
12
Sample

Zone	Thin sections	Flurescence thin sections	2D map by NMR tests	Oil contents, $\mu l \cdot g^{-1}$	S_{o1} $mg \cdot g^{-1}$
High-grade metamorphic zone	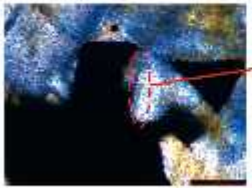		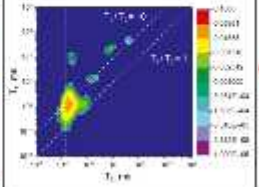	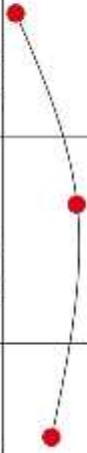	
Low-grade metamorphic zone			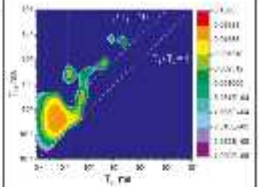		
None metamorphic zone	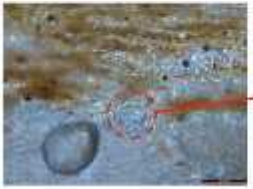		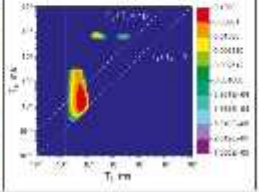		

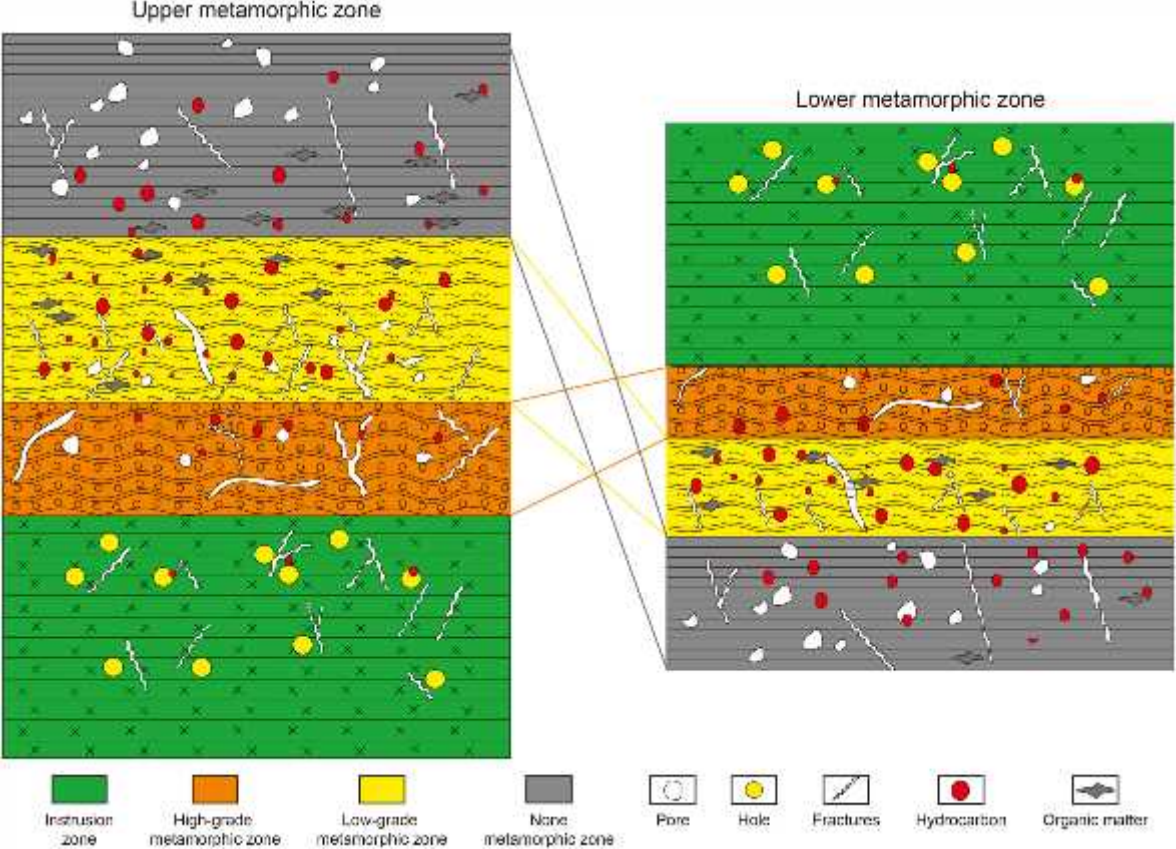
Upper metamorphic zone
Lower metamorphic zone
Instrusion zone
High-grade metamorphic zone
Low-grade metsmorphic zone
None metamorphic zone
Pore
Hole
Fractures
Hydrocarbon
Organic matter

Declaration of interests

The authors declare that they have no known competing financial interests or personal relationships that could have appeared to influence the work reported in this paper.

The authors declare the following financial interests/personal relationships which may be considered as potential competing interests: